Distal Pocket Polarity in Ligand Binding to Myoglobin: Structural and Functional Characterization of a Threonine^{68}(E11) Mutant†

Stephen J. Smerdon, Guy G. Dodson, and Anthony J. Wilkinson*
Department of Chemistry, University of York, Heslington, York YO1 5DD, U.K.
Quentin H. Gibson and Richard S. Blackmore
Department of Biochemistry and Molecular and Cell Biology, Cornell University, Ithaca, New York 14853
Theodore E. Carver and John S. Olson
Department of Biochemistry and Cell Biology, Rice University, Houston, Texas 77251
Received January 11, 1991; Revised Manuscript Received March 20, 1991

ABSTRACT: Site-directed mutagenesis studies have confirmed that the distal histidine in myoglobin stabilizes bound O_2 by hydrogen bonding and have suggested that it is the polar character of the imidazole side chain rather than its size that limits the rate of ligand entry into the protein. We constructed an isosteric Val^{68} to Thr replacement in pig myoglobin (i) to investigate whether the O_2 affinity could be increased by the introduction of a second hydrogen-bonding group into the distal heme pocket and (ii) to examine the influence of polarity on the ligand binding rates more rigorously. The 1.9-Å crystal structure of Thr^{68} aquomet-myoglobin confirms that the mutant and wild-type proteins are essentially isostructural and reveals that the β-OH group of Thr^{68} is in a position to form hydrogen-bonding interactions both with the coordinated water molecule and with the main chain >C=O of residue 64. The rate of azide binding to the ferric form of the Thr^{68} mutant was 60-fold lower than that for the wild-type protein, consistent with the proposed stabilization of the coordinated water molecule. However, bound O_2 is destabilized in the ferrous form of the mutant protein. The observed 17-fold lowering of the O_2 affinity may be a consequence of the hydrogen-bonding interaction made between the Thr^{68} β-OH group and the carbonyl oxygen of residue 64. Overall association rate constants for O_2, NO, and alkyl isocyanide binding to ferrous pig myoglobin were 3–10-fold lower for the mutant compared to the wild-type protein, whereas that for CO binding was little affected. Time courses for intramolecular rebinding of these ligands were measured following 17-ns and 35-ps laser excitation pulses. In each case, the quantum yields were lowered and the rate constants for rebinding were increased. For oxygen, nanosecond time courses were fitted to a two-step consecutive reaction scheme. Although the Thr^{68} hydroxyl group caused both the inner and outer kinetic barriers to be raised, its major effect was to raise the free energy of the intermediate state with O_2 noncovalently bound in the distal pocket. These observations demonstrate unambiguously that the polarity of the distal heme pocket is an important determinant of the rate of ligand binding presumably through its influence on the stability of noncovalently bound water in deoxymyoglobin.

X-ray crystallographic data have provided the framework for interpreting the functional roles of key amino acid side chains surrounding the O_2 binding sites in mammalian hemoglobins and myoglobins. In 1962, Pauling proposed that the distal histidine [His^{64}(E7)] stabilized the bound O_2 through the formation of a hydrogen bond between the imidazole and the second bound oxygen atom. This idea is supported by the high-resolution X-ray structure of sperm whale oxymyoglobin and neutron diffraction data for the same protein (Phillips, 1980 & 1981; Phillips & Schoenborn, 1981). Perutz and Matthews (1966) noted that this same residue, His(E7), blocks direct access from the solvent to the heme iron atom in both myoglobin and hemoglobin and probably comprises a major portion of the kinetic barrier to ligand binding. Molecular dynamics simulations have refined this latter idea and suggested that ligands gain entry into myoglobin through a channel that forms transiently by movements of the side chains of His^{64} and Val^{68}(E11) (Case & Karplus, 1979; Kottalam & Case, 1988). The proposed rotations of the distal histidine do take place when large ligands are bound to the heme iron atom (Bolognesi et al., 1982; Ringe et al., 1984; Kuriyan et al., 1986; Johnson et al., 1989).

Since the X-ray structures are so compelling, the mechanisms proposed from these data are often accepted without quantitative testing. In the last five years, the development of globin expression systems and site-directed mutagenesis has provided the technology for evaluating in much greater detail the functional significance of specific structural features in hemoglobin and myoglobin (Nagai & Thøgersen 1984; Varadarajan et al., 1985; Springer & Sligar, 1987; Dodson et al., 1988). For example, the distal histidine in sperm whale myoglobin has been replaced by 12 different amino acids, and the overall and geminate ligand binding parameters for most of these mutants have been measured in detail (Springer et al., 1989; Rohlfs et al., 1990; Carver et al., 1990).

Although for the most part these mutagenesis studies have supported previous ideas about the role of this residue in oxygen binding, a number of surprising results were obtained. Substitution of the distal histidine always caused a decrease

†This research was supported by Grant GR/E 98867 from the Science and Engineering Research Council, U.K. (G.G.D. and A.J.W.), by United States Public Health Service Grant GM-14276 (Q.H.G.), by United States Public Health Service Grant GM-35649 (J.S.O.), Grant C-612 from the Robert A. Welch Foundation (J.S.O.), and Grant 4073 from the Advanced Technology Program of the Texas Higher Education Coordinating Board (J.S.O.). T.E.C. is the recipient of a graduate fellowship from the National Institutes of Health, Training Grant GM-07933 from the National Institute of Medical Science.

0006-2960/91/0430-6252$02.50/0

in O_2 affinity even in the case of the His^{64} to Gln substitution, which gave a 6-fold decrease, the smallest effect (Rohlfs et al., 1990). These results are consistent with the idea that the hydrogen bond between His^{64} and bound O_2 lowers the free energy of binding by 1–2 kcal/mol. Replacement of His^{64} with apolar residues also caused 5–10-fold increases in the bimolecular rate constants for CO and O_2 binding, and this effect was roughly independent of the size of the amino acid for the series Gly, Val, Leu, Phe. In contrast, the association rate constants for CO and O_2 binding to the Gln^{64} mutant were only slightly elevated (<2-fold). These results suggested that the polar nature, not the size, of the imidazole side chain causes inhibition of ligand entry into the heme pocket. This polarity effect was explained in terms of stabilization of noncoordinated water within the distal pocket of deoxymyoglobin since these water molecules must be displaced when ligands approach the heme iron atom (Rohlfs et al., 1900; Carver et al., 1990). Similar polarity effects have been used to explain the solvent dependence of ligand binding to model heme compounds [see Traylor et al. (1985) and Springer et al. (1989), and references therein).

There are, however, two major problems with these previous mutagenesis studies. First, none of the mutations at residue 64 was isosteric so that alterations in the conformation of the heme pocket could, in principle, account for the changes in O_2 binding parameters without having to invoke polarity arguments. Second, all of the substitutions caused increases in the association rate constants and decreases in O_2 affinity. Elber and Karplus (1990) have suggested that these "mutant experiments can be regarded as analogous to making a hole in a tire, from which one cannot conclude that the air normally comes out of (or goes into) the hole rather than the valve". Regardless of the applicability of this metaphor, it is clear that more definitive interpretations could be made for substitutions that cause a lowering of the observed association rates and/or an increase in affinity.

In order to address these problems and to test the importance of polar interactions, we have constructed a mutant pig myoglobin in which the distal valine is replaced by threonine. Threonine and valine are isosteric so that the influence of polarity may be examined without significant alteration of the volume of the distal pocket. Furthermore, van der Waals' interactions made by the isopropyl side chain of the valine with other groups in the protein will be preserved. This substitution provides an unequivocal test of the importance of polarity in determining the rates of ligand binding. In principle, the β-hydroxyl of Thr^{68} should further stabilize noncovalently bound water in the distal pocket of deoxymyoglobin, causing decreases in the rates of ligand entry into the protein. We were also curious to investigate whether the introduction of a second hydrogen-bonding group in the distal pocket would further stabilize bound O_2, causing an increase in affinity. Consequently, the wild-type and Thr^{68} mutant myoglobins have been extensively characterized with use of a combination of techniques. We have determined the crystal structure of Thr^{68} aquometmyoglobin at 1.9-Å resolution. Stopped-flow rapid-mixing methods and conventional flash photolysis data were combined to determine the overall rates of binding of azide, oxygen, carbon monoxide, nitric oxide, and a series of alkyl isocyanides. Finally, nano- and picosecond flash photolysis techniques were used to follow the recombination of ligands with the iron from within the protein.

Materials and Methods

Protein Preparation. The construction of an expression system for recombinant pig myoglobin has been described previously (Dodson et al., 1988). For mutagenesis, the pig myoglobin coding sequence was subcloned into the phagemid vector pBluescript-KS+ (Stratagene Inc.). The oligonucleotide 5′-GCAACACGACGCTGACTG-3′ (where bold characters denote mismatches) was used to direct the replacement of the codon GTG for $valine^{68}$ with the codon ACG for threonine with use of standard techniques (Zoller & Smith, 1983). For expression of wild-type and mutant myoglobins, the coding sequence was subcloned in the plasmid pLcII (Nagai & Thøgersen, 1984) and introduced into the temperature-sensitive λ lysogen *Escherichia coli* M5219 (Remaut et al., 1981). Mutant and wild-type recombinant myoglobins were expressed as fusion proteins following induction and reconstituted with heme, and the fusion portion was removed by proteolytic digestion with trypsin. It has been established that native pig heart and recombinant pig myoglobin purified from *E. coli* exhibit identical ligand binding kinetics (Carver et al., 1991).

Crystallography: Data Collection and Processing. Crystals of Thr^{68} myoglobin were grown from 70% ammonium sulfate in potassium phosphate buffer, pH 7.1, as described for wild-type metmyoglobin (Dodson et al., 1988). Diffraction data were collected to 1.9-Å spacing from a single crystal at the synchrotron radiation source at the EMBL outstation at DESY (station X31, λ = 1.06 Å), Hamburg, with use of a Fuji imaging plate detector. The data were collected as two sets. Initially, all reflections were measured over a rotation range of 100° about the c^* axis in 2° oscillations with a crystal-to-detector distance of 166 mm. Under these conditions, many of the low-resolution terms were saturated. These data were rescued by collecting a second data set over the same rotation range but with use of an oscillation angle of 5° and a crystal-to-detector setting of 303 mm. Reflections were indexed in space group $C2$, and crystal missetting and unit-cell parameters were determined by use of the program REFIX (Kabsch, 1988). Reflections were integrated with use of a version of the MOSFLM film processing package adapted for the image plate. Oblique incidence, Lorentz, and polarization corrections were calculated and applied. Scale and temperature factors for each batch were calculated in the standard CCP4 version of ROTAVATA. Scale factors were applied and partial reflections were summed with use of the program AGROVATA (CCP4, 1986). A total of 66 671 observations of 31 650 unique reflections were made in the high-resolution data set. These data gave a merging R-factor on intensities of 10.4% and a mean$(I)/\sigma(I)$ of 6.85. For the low-resolution set, 18 670 measurements of 8790 unique reflections were made, which gave a merging R-factor of 4.8% on intensities with a mean$(I)/\sigma(I)$ of 14.7. After the high- and low-resolution data sets were merged, 91.6% of all reflections to 1.9 Å were represented. Finally, the data were reindexed in the nonstandard monoclinic space group $I2_1$. The $I2_1$ unit-cell parameters are a = 123.8 Å, b = 42.5 Å, c = 92.1 Å, and β = 92.1°.

Structure Refinement. The Thr^{68} myoglobin structure was initially refined by use of restrained molecular dynamics (Brunger, 1988) employing the program X-PLOR version 1.5 implemented on an ALIANT FX40 mini-supercomputer. The starting model was the wild-type myoglobin structure refined (R = 18.6%) against 2.5-Å data (Smerdon et al., 1990) with the side chain of Val^{68} truncated to Cβ in the two molecules of the asymmetric unit. This procedure reduced the starting R-factor (40.9%) to 25.2%. Subsequent refinement was carried out by use of iterative cycles of restrained reciprocal space least-squares refinement (Hendrickson & Konnert, 1980) punctuated with three interactive molecular model building sessions using the program FRODO (Jones, 1978). The final

R-factor after the addition of atoms for the Thr[68] side chains for the structure containing 106 water and 2 sulfate molecules is 20.7% for all data between 7 and 1.9 Å (34 782 reflections representing 98.5% of all the data collected). The root mean square deviation from bond length ideality is 0.027 Å, and the average of the individual atomic *B*-factors is 23.9 Å^2.

Kinetic Measurements. Overall association and dissociation rate constants were measured with use of stopped-flow rapid-mixing and conventional flash photolysis techniques as described by Rohlfs et al. (1990). Equilibrium constants were calculated from the ratio of the rate constants. Under pseudo-first-order conditions, wild-type and Thr[68] pig myoglobins showed monophasic, exponential time courses. The absence of conformational heterogeneity on millisecond time scales was also confirmed by comparing association rate constants measured in both rapid-mixing and conventional flash photolysis experiments [see Egeberg et al. (1990)].

Nanosecond and picosecond photolysis experiments were carried out in 0.1 M potassium phosphate, pH 7.0, 20 °C, as described by Carver et al. (1990). For the measurement of time courses with half-times greater than 10 ns, a Phase-R 2100B dye laser was used to generate rectangular 17-ns pulses in cavity-dump mode operation with a switching time of less than 2 ns. Absorbance data were collected at 436 nm for O_2, CO, and NO complexes and at 445 nm for the isocyanide complexes using a Hamamatsu photomultiplier attached to a Tektronix Model 7104 oscilloscope that in turn was interfaced to an IBM AT computer. For the faster picosecond reactions, a Nd-Yag active–passive mode-locked laser (Quantel Model YG571) was used to generate 35-ps pulses at 1064 nm that were frequency doubled to 532 nm for the excitation pulse. The observation pulse was Raman shifted to 436 nm. Pulse–probe data collection was performed as described by Carver et al. (1990).

For each of the ligands the observed time courses were fitted to schemes comprised of the minimum number of substates. Time courses for picosecond NO recombination were heterogenous and could be fitted satisfactorily to sequential or parallel reaction schemes of the form

$$\begin{array}{ccc} A \rightleftharpoons B_1 \rightleftharpoons B_2 & & A_1 \rightleftharpoons B_1 \\ & & \updownarrow \\ & & A_2 \rightleftharpoons B_2 \end{array} \qquad (1)$$

where A, A_1, and A_2 represent equilibrium-bound states. The exact structural character of the intermediate states is unknown; however, the B states have been interpreted as iron–ligand contact pairs where the photodissociated NO is within 1 or 2 van der Waals' radii of the iron atom (Jongeward et al., 1988; Carver et al., 1990). In the linear scheme, multiple intermediates are generated by sequential movements of the ligand away from the iron atom; in the parallel mechanism the different geminate rates arise from either multiple ground-state conformations or from decay of a common excited-state species into two different geminate states (Doster et al., 1982; Petrich et al., 1988; Jongeward et al., 1988). For consistency with previous interpretations, the NO recombination time courses were fitted to the sequential scheme by integrating the corresponding differential equations both during and after the 35-ps excitation pulse (Carver et al., 1990).

The O_2 and methyl and ethyl isocyanide complexes of native and Thr[68] pig myoglobin showed no picosecond processes following a 35-ps light pulse. Slower nanosecond processes ($t_{1/2}$ = 1.5–30 ns) were evident in the pulse–probe time courses; however, since data could only be collected out to 1500 ps, the best values of the rates of O_2 and isocyanide recombination were obtained with the nanosecond dye laser system. Nanosecond time courses for the geminate recombination of these ligands were generated with use of a 17-ns light pulse and were evaluated in terms of a simplified two-step scheme (eq 2), in

$$\mathrm{MbX\ or\ A} \underset{k_{hv}Q_{ni}I(t)+\,k_{AC}}{\overset{k_{CA}}{\rightleftharpoons}} [C_1 \rightleftharpoons C_2] \overset{k'_{XC}}{\underset{k_{CX}}{\rightleftharpoons}} \mathrm{Mb + X} \qquad (2)$$

which C represents a state in which the ligand is farther removed from the iron (relative to B) and noncovalently bound in the distal heme pocket and Mb + X is deoxymyoglobin with the ligand free in solution. The bimolecular rate constant for the formation of state C can be computed from the value of the overall association rate constant, k', with use of the formula $k'_{XC} = k'(k_{CA} + k_{CX})/k_{CA}$. Similarly, the rate of thermal iron–ligand bond breakage can be calculated from $k_{AC} = k(k_{CA} + k_{CX})/k_{CX}$, where k is the overall dissociation rate constant. The nanosecond time courses for O_2 rebinding to wild-type and Thr[68] pig myoglobin were monophasic, indicating a single C substate and were fitted to eq 2 with use of data collected at different light intensities (Gibson et al., 1986; Carver et al., 1990). Monophasic time courses were also observed for methyl and ethyl isocyanide rebinding to native pig myoglobin. Biphasic traces were observed for isocyanide recombination with the Thr[68] mutant and analyzed in terms of two consecutive C substates, C_1 and C_2 in eq 2.

In common with other authors, we have assumed that the geminate picosecond, geminate nanosecond, and bimolecular millisecond reactions are interconnected according to the consecutive scheme A ⇌ B ⇌ C ⇌ Mb + X. Thus, the lack of measurable picosecond processes for O_2 and isocyanide time courses implies that the rate of recombination with the iron from the contact pair is much slower than the rate of migration from state B to state C, i.e., $k_{BA} \ll k_{BC}$.

Results

Crystal Structure of Thr[68] Metmyoglobin. The structure of Thr[68] aquometmyoglobin shows very few differences from the structure of the wild-type protein refined against 1.8-Å data[1,2] (T. J. Oldfield et al., manuscript in preparation) as was expected from the isosteric character of the mutation. A least-squares overlap of Thr[68] myoglobin main-chain atoms with those of the wild-type structure shows root mean square deviations of 0.3 Å for both the A molecule and the B molecule individually. If both molecules of the asymmetric unit are overlapped together, this deviation rises to 0.5 Å. This reflects a small change in the relative orientation of the molecules of the asymmetric unit in the mutant crystals and accounts for the high initial *R*-factor prior to refinement (41%). Superposition of the A and the B molecules of the asymmetric unit of the mutant crystal yields an rms deviation of 0.2 Å in all main-chain atoms.

Electron density associated with the environment of the heme group in the A molecule is shown in Figure 1, and a least-squares overlap of the mutant and wild-type structures in this region is presented in Figure 2. There is close similarity

[1] In the wild-type 2.5-Å metmyoglobin structure no density was observed for a liganded water molecule at the sixth coordination position at the iron (Smerdon et al., 1990). Unlike in the 2.5-Å structure, in the 1.8-Å structure of this protein refined against data collected on a second crystal unambiguous density for a coordinated water molecule is observed and similar density is seen in structures of two position 45 (CD3) mutant pig aquometmyoglobins at similar resolution (T. J. Oldfield et al., manuscript in preparation).

[2] Coordinates will be deposited in the Brookhaven Protein Data Bank.

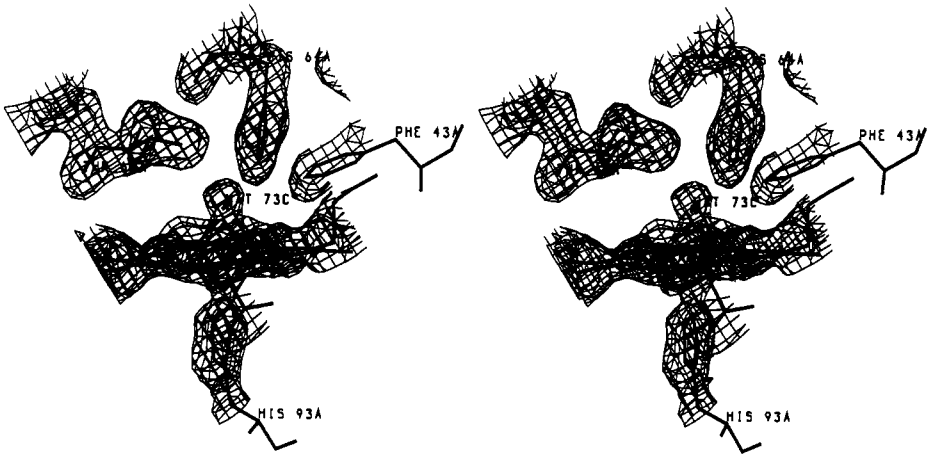

FIGURE 1: Stereo pair of the electron density in the region of the heme pocket in the A molecule of the Thr^{68} myoglobin structure. The view is from the back of the pocket. The figure shows the density associated with the distal residues Phe^{43}, His^{64}, and Thr^{68}, the proximal His^{93}, and the heme group with the coordinated water molecule (WAT 73C). The electron density is contoured at 0.6 eÅ^{-3}.

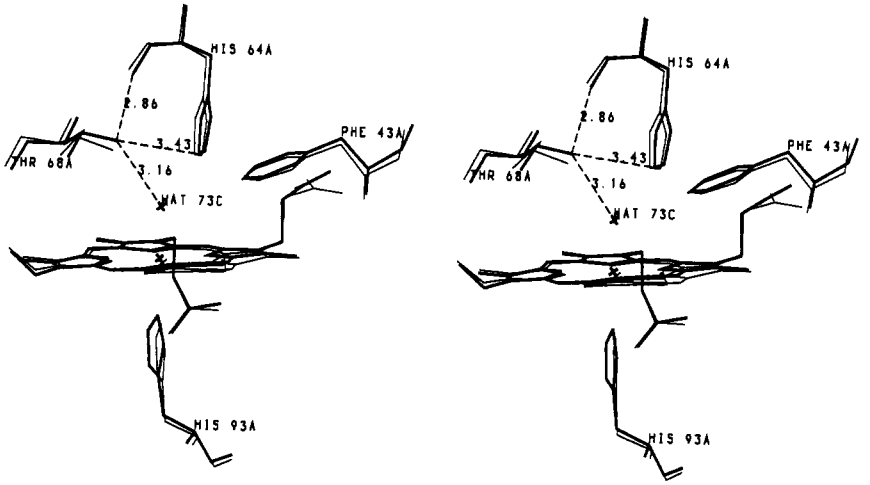

FIGURE 2: Superposition of the heme and surrounding residues in Thr^{68} myoglobin (thick lines) with those of the wild-type protein (thin lines). The view is from the back of the distal pocket. A least-squares overlap was performed on all main-chain atoms between residues 2 and 150 in the A molecules of the respective asymmetric units. The distances of separation in angstroms of the liganded water molecule, N_ϵ of the distal His^{64}, and the main-chain carbonyl oxygen of His^{64} from the hydroxyl oxygen of the threonine are indicated.

between the structures in the distal pocket; the principal difference is that the oxygen of the Thr^{68} side chain is 0.5 Å closer to the carbonyl oxygen of His^{64} in the mutant structure relative to the γ2 methyl carbon of Val^{68} in the wild-type structure. This is brought about mainly by a rotation of the position 68 side chain about its C_α–C_β bond, together with a small shift in the position of the main-chain carbonyl oxygen. At 2.9-Å separation, a favorable hydrogen-bonding interaction is possible between these groups. The threonine hydroxyl may also form a hydrogen bond with the coordinated water molecule (WAT 73C) in the aquomet form of the mutant (Figures 1 and 2). Similar displacements and interactions are seen in the B molecule.

Overall Ligand Binding Parameters. The Val^{68} to Thr mutation caused 4–6-fold decreases in the association rate constants for NO, O_2, and isocyanide binding, whereas this substitution produced little change in k' for CO binding (Table I and Figure 3). These results provide a striking example of the differences between CO binding, which is known to be limited by the rate of intramolecular bond formation, and NO, O_2, and isocyanide binding, which are limited partly or completely by the rate of ligand movement into the heme pocket (Carver et al., 1990, and references therein). The rate constants for O_2 and CO dissociation from Thr^{68} myoglobin were 3–4-fold greater than those for the wild-type protein. As a result, the affinities of the mutant protein for O_2 and CO were 17- and 5-fold smaller, respectively, than those for native myoglobin. In contrast to the gases, the isocyanide dissociation rate constants decreased to roughly the same extent as the

Table I: Overall Kinetic Parameters for Ligand Binding to Val^{68} (Wild-Type) and Thr^{68} Pig Myoglobin at 20 °C, pH 7[a]

protein	ligand	k' (μM^{-1} s^{-1})	k (s^{-1})	K (μM^{-1})
Val^{68} (wild type)	NO	17		
	O_2	17	14	1.2
	CO	0.78	0.019	41
	MNC	0.11	4.4	0.025
	ENC	0.098	0.64	0.15
	nPNC	0.061	0.70	0.087
	nBNC	0.040	0.5	0.080
Thr^{68}	NO	4.9		
	O_2	2.8	39	0.072
	CO	0.61	0.079	7.7
	MNC	0.039	1.2	0.033
	ENC	0.018	0.092	0.20
	nPNC	0.0095	0.082	0.12
	nBNC	0.0088	0.16	0.056

[a] The association, k', and dissociation, k, rate constants for Val^{68} myoglobin were computed as the mean of those obtained for wild-type protein produced in *E. coli* and for native pig myoglobin [see Carver et al. (1991). The isocyanide abbreviations are MNC, methyl; ENC, ethyl; nPNC, *n*-propyl; and nBNC, *n*-butyl. On the basis of similar measurements with sperm whale myoglobin, a relative error of ±20% is assumed to apply to the kinetic parameters for pig myoglobin (Rohlfs et al., 1990).

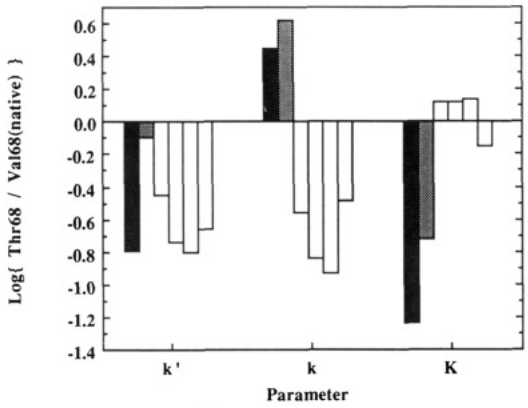

FIGURE 3: Effect of the Val[68] to Thr mutation on the overall rate and equilibrium constants for O_2 (solid bars), CO (shaded bars), and alkyl (open bars, from left to right for methyl, ethyl, *n*-propyl, and *n*-butyl) isocyanides binding to pig myoglobin at pH 7, 20 °C. The logarithm of the ratio of the mutant to wild type parameter is given on the *y*-axis. k', k, and K represent the overall association rate, dissociation rate, and equilibrium association constants, respectively.

Table II: Azide Binding Parameters for Mutants of Ferric Pig Myoglobin at 20 °C in 0.1 M Phosphate, pH 7[a]

substitution	k' (x10^{-3} M^{-1} s^{-1})	k (s^{-1})	K (x10^{-3} M^{-1})
native	7.6	0.14	54
Thr[68]	0.12	0.8	0.15
Arg[45]	3.7	0.064	58
sperm whale	3.3	0.11	30

[a] Association reactions were carried out in the stopped-flow apparatus by mixing NaN_3 with 5 μM metmyoglobin and following the absorbance changes at 405 nm. Dissociation reactions were followed by replacing bound azide in the presence of excess NaCN.

Table III: NO Rebinding to Val[68] (Native) and Thr[68] Pig Myoglobin following a 30-ps Laser Excitation Pulse at 20 °C, pH 7.0[a]

protein	Q_{ps} (ns^{-1})	k_{B_1A} (ns^{-1})	$k_{B_1B_2}$ (ns^{-1})	$k_{B_2B_1}$
Val[68]	0.20 ± 0.03	14 ± 3	6 ± 2	3 ± 1
Thr[68]	0.10 ± 0.02	50 ± 10	7 ± 2	4 ± 2

[a] The errors for the Val[68] (wild type) and Thr[68] parameters were calculated as the standard deviation from the mean computed from three and six independent experiments, respectively. A linear consecutive reaction scheme was used to fit the data, assuming two B states. The time courses could also be fitted to a parallel scheme in which 88% of the recombination occurred with a rate constant of 57 × 10^9 s^{-1} and 12% with a rate constant equal to 4 × 10^9 s^{-1} for the Thr[68] mutant and 82% of the recombination occurred with a rate constant of 20 × 10^9 s^{-1} and 18% with a rate constant of 3 × 10^9 s^{-1} for Val[68] (native) pig myoglobin. Q_{ps} is the apparent picosecond quantum yield of geminate B states, which was obtained with use of the fitting procedures described by Carver et al. (1991).

corresponding association rate constants, and as a result, the affinity of pig myoglobin for these ligands was little affected by the Thr[68] mutation.

The Val[68] to Thr mutation caused a 60-fold decrease in the rate of azide binding to the ferric form of pig myoglobin (Table II). The azide dissociation rate constant is increased 5–6-fold, resulting in a 360-fold lowering in azide affinity. Native pig myoglobin shows a 2-fold greater rate of azide binding than sperm whale myoglobin. This difference appears to be due to the residue at position 45, which is Lys in the case of the pig protein and Arg in the case of the whale myoglobin. As shown in Table II, substitution of Arg for Lys[45] in pig myoglobin causes k' for azide binding to decrease to the value observed for the native sperm whale protein.

Geminate Recombination Reactions. Comparisons of the geminate parameters for NO, O_2, CO, methyl isocyanide, and

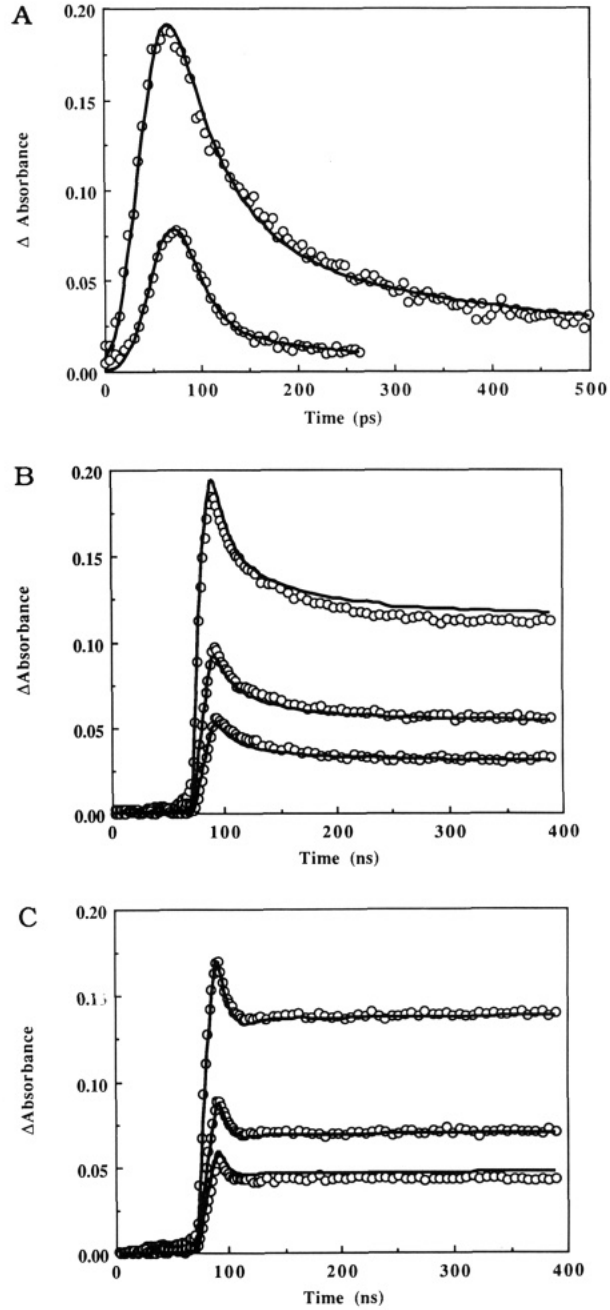

FIGURE 4: Time courses for the geminate recombination of NO and O_2 with wild-type and Thr[68] pig myoglobin at 20 °C, pH 7. Panel A: Time courses for NO rebinding during and after a 35-ps excitation pulse at a relative light intensity of $^1/_4$ full flash. The wavelength of observation was 436 nm. The maximum expected absorbance changes for both samples were 0.7–0.8. The open circles represent observed data and the solid lines fits to eq 1 (see Table III). The smaller absorbance excursion for the Thr[68] mutant (lower trace) relative to the wild-type (upper trace) myoglobin is due to both a larger value of k_{B_1A} and a smaller value of Q_{ps}. Panels B and C: Time courses for O_2 rebinding to wild-type (panel B) and Thr[68] myoglobin (panel C) during and after a 17-ns flash. The open circles represent observed data at excitation intensities (top to bottom) of $^1/_8$, $^1/_{32}$, and $^1/_{64}$ full laser light for wild-type pig oxymyoglobin and $^1/_4$, $^1/_8$, and $^1/_{16}$ for the Thr[68] protein. The maximum expected absorbance changes at 436 nm in these experiments were 0.24 (wild type) and 0.29 (Thr[68]). The solid lines represent fits to eq 2 with use of the parameters listed in Table IV.

ethyl isocyanide rebinding to native and Thr[68] pig myoglobin are shown in Tables III–VI. The NO time courses were dominated by large picosecond phases (Figure 4A); O_2 and isocyanide rebinding occurred only on nanosecond time scales (Figure 4B,C), and little CO recombination was observed on

Table IV: O_2 Rebinding to Val^{68} (native) and Thr^{68} Pig Myoglobin following a 17-ns Laser Pulse at 20 °C, pH 7.0[a]

protein	k'_{XC} (μM^{-1} s^{-1})	k_{CX} (μs^{-1})	K_{XC} (M^{-1})	k_{CA} (μs^{-1})	k_{AC} (s^{-1})	K_{CA} (x10^{-6})	Q_{ns}
Val^{68}	33	15	2.2	17	30	0.57	0.13
Thr^{68}	5.2	63	0.082	75	85	0.88	0.05

[a] The nanosecond processes were assigned to the C state in eq 2; no picosecond geminate recombination processes were observed for these proteins. Observed time courses were fitted to eq 2 as described by Carver et al. (1990). Comparisons of observed and computed curves are shown in Figure 4. Q_{ns} is the fitted quantum yield for the photochemical production of nanosecond geminate intermediates.

Table V: Estimate of CO Geminate Rebinding Parameters for Native Sperm Whale, Wild-Type Pig, and Thr^{68} Pig Myoglobin at 20 °C, pH 7[a]

protein	k' (μM^{-1} s^{-1})	K_{XC} (M^{-1})	k_{CA} (μs^{-1})	k_{AC} (s^{-1})	K_{CA}
sperm whale Val^{68} (native)	0.51	2.2	0.24	0.019	13
pig Val^{68} (native)	0.78	2	0.4	0.019	21
pig Thr^{68}	0.61	0.1	6	0.079	76

[a] The equilibrium constant for noncovalent CO binding, K_{XC}, and the rate of iron–ligand bond formation, k_{CA}, for sperm whale myoglobin were taken from Henry et al. (1983) [see Carver et al. (1990)]. K_{XC} values for noncovalent CO binding to wild-type and Thr^{68} pig myoglobins were assumed to be equal to the corresponding values for O_2 binding shown in Table IV. k_{CA} values for CO rebinding to the pig myoglobins were calculated from $k_{CA} = k'/K_{XC}$.

any time scale (≤10% recombination). Two general trends were observed. First, the picosecond, nanosecond, and overall quantum yields of the Thr^{68} mutant were consistently smaller than those for the wild-type protein. This was also true for the CO complex of Thr^{68} myoglobin where the overall quantum yield with a 0.5-ms excitation pulse was measured to be 0.7, even though no more than 10% of the photolyzed CO recombined geminately. Thus, the mutation has a significant effect on the photophysical processes involved in iron–ligand bond breakage and inhibits the formation of geminate intermediates. Second, the rate constants for ligand rebinding from the observed geminate states, k_{BA} and k_{CA} in eqs 1 and 2, were uniformly larger than those for the wild-type protein. This result indicates that the kinetic barrier for intramolecular iron–ligand bond formation has been lowered and/or that the geminate intermediates are less stable in the mutant protein.

In the case of O_2 binding, the rate constant for ligand entry into the Thr^{68} mutant, k'_{XC}, decreased 6-fold compared to native myoglobin, whereas the rate constant for escape from the heme pocket, k_{CX}, increased 4-fold. The net result of these changes is a 27-fold decrease in the equilibrium constant for O_2 occupancy of the distal cavity. This result supports our previous suggestion that the first step in O_2 binding may involve the displacement of water, which is hydrogen bonded to His^{64} in the distal pocket of deoxymyoglobin (Phillips, 1981; Rohlfs et al., 1990; Carver et al., 1990). The addition of another polar group in the Thr^{68} mutant probably stabilizes this distal pocket water further, inhibiting its displacement by apolar ligands.

Estimates of k_{CA} for CO rebinding were obtained by assuming that K_{XC} for CO is similar to that measured for O_2 binding. Rohlfs et al. (1988) and Carver et al. (1990) have shown that, within a factor of 2–3, this assumption is valid for a variety of naturally occurring monomeric heme proteins and at least two different distal pocket mutants of sperm whale myoglobin. At room temperature in aqueous solvents, the association rate constant for CO binding to myoglobin is given by $k'_{CO} = K_{XC}k_{CA}$ (Doster et al., 1982; Henry et al., 1983; Gibson et al., 1986). Values of k_{CA} for CO binding to wild-type and Thr^{68} pig myoglobin were calculated with use of this formula, the k'_{CO} values in Table I, and the K_{XC} values for O_2 binding in Table IV. The resultant parameters are compared in Table V to those measured directly for CO rebinding to sperm whale myoglobin by Henry et al. (1983). This computation indicates that the Val^{68} to Thr substitution produces a 15-fold increase in k_{CA} for CO binding, which offsets the decrease in K_{XC}, providing an explanation for the lack of effect on k'_{CO} (Figure 3). To test this conclusion, direct measurements of CO rebinding were made for Thr^{68} myoglobin by averaging repetitively large numbers of traces following a 9-ns flash from the Nd-Yag laser. Roughly 10% recombination was observed with a geminate rate of $\sim 3.5 \times 10^7$ s^{-1}. These results gave estimates for k'_{XC}, k_{CX}, K_{XC}, and k_{CA} equal to roughly 4×10^6 M^{-1} s^{-1}, 3×10^7 s^{-1}, 0.1 M^{-1}, and 5×10^6 s^{-1}, respectively, which agree well with the computed values in Table V.

Monophasic time courses were also observed for methyl and ethyl isocyanide rebinding to wild-type pig myoglobin and analyzed as described for O_2 rebinding (Table VI, part A). Biphasic nanosecond time courses were observed for isocyanide rebinding to Thr^{68} myoglobin, and these data were analyzed in terms of a three-step, consecutive reaction scheme based on eq 2 ($A \rightleftharpoons C_1 \rightleftharpoons C_2 \rightleftharpoons X + Mb$; Table VI, part B). In spite of this additional complexity, the effects of the Thr^{68} mutation on methyl and ethyl isocyanide rebinding are basically the same as those observed for O_2 and CO rebinding. The rate of iron–ligand bond formation, k_{C_1A} or k_{CA}, increased 2-fold and the equilibrium constant for the migration of these ligands into the distal pocket, K_{XC} or $K_{XC_2}K_{C_2C_1}$, decreased markedly (7–8-fold) when Val^{68} was replaced with Thr (Table

Table VI: Methyl and Ethyl Isocyanide Rebinding to Val^{68} (native) and Thr^{68} Pig Myoglobin at 20 °C, pH 7.0[a]

A. Rate Parameters for native (Val^{68}) Pig Myoglobin

ligand	k'_{XC} (μM^{-1} s^{-1})	k_{CX} (μs^{-1})	K_{XC} (M^{-1})	k_{CA} (μs^{-1})	k_{AC} (μs^{-1})	K_{CA}	Q_{ns}
MNC	0.14	9.3	0.015	36	21	1.7	~1
ENC	0.12	22	0.0052	130	4.3	30	~1

B. Rate Parameters for Thr^{68} Pig Myoglobin[b]

ligand	k'_{XC_2} (μM^{-1} s^{-1})	k_{C_2X} (μs^{-1})	K_{XC_2} (M^{-1})	$k_{C_2C_1}$ (μs^{-1})	$k_{C_1C_2}$ (μs^{-1})	$K_{C_2C_1}$	k_{C_1A} (μs^{-1})	k_{AC_1} (s^{-1})	K_{C_1A}	Q_{ns}
MNC	0.16	8.2	0.019	4.2	38	0.11[b]	68	4.4	15	0.63
ENC	0.023	2.3	0.010	12	160	0.074[b]	280	1.1	260	0.67

[a] For wild-type pig myoglobin, only a single phase was observed and only one C state (eq 2) was defined. For the Thr^{68} mutant, two phases were observed on the nanosecond time scales and were assigned to multiple C states by fitting time courses collected at five different light intensities following a 17-ns laser flash [see Carver et al. (1990)]. [b] Note that the effective equilibrium constant for noncovalent binding to state C_1 in the Thr^{68} mutant is given by $K_{XC_2}K_{C_2C_1}$ and is roughly 10-fold smaller than K_{XC} for isocyanide binding to the wild-type protein. Thus, as in the case of O_2 binding, the stability of these isocyanides in the distal pocket is greatly reduced by the Val^{68} to Thr mutation.

VI). These conclusions apply even if a parallel reaction scheme is adopted to analyze the biphasic time courses for the mutant protein. For both isocyanides, the fitted parameters for Thr^{68} myoglobin suggest a major intermediate (roughly 64% of the absorbance change when pumping during the 17-ns light pulse is taken into account) that has much larger rate constants for intramolecular rebinding and ligand escape than those observed for the wild-type protein.

Discussion

Polar Interactions in the Distal Pocket. The isosteric character of the Val^{68} to Thr mutation means that the interpretation of ligand binding data is a priori uncomplicated by differences in the size or the stereochemistry of the side chains at position 68. The close similarity of the Thr^{68} myoglobin structure to the wild-type structure argues strongly that the large functional differences between these proteins are due to the polarity of the Thr^{68} side chain.

Giacometti et al. (1981a,b) and others have suggested that the rate of azide binding to metmyoglobin is a measure of the stability of the coordinated water molecule that must be displaced from the iron atom before the ligand can bind. These workers showed that the association rate constant for azide binding to *Aplysia limacina* myoglobin is 1000-fold greater than that for sperm whale myoglobin at pH 6, 20 °C. This large difference correlates with spectroscopic measurements, which suggest that water is not coordinated with the ferric iron atom in *Aplysia* myoglobin at low pH. The lack of bound water was attributed to the apolar nature of the distal pocket in the *Aplysia* protein where the E7 and E11 residues are Val^{63} and Ile^{67}, respectively (Bolognesi et al., 1989). As shown in Table II, the Val^{68} to Thr substitution in pig myoglobin produced an effect that was the opposite of that observed for *Aplysia* myoglobin. This mutation caused a 60-fold decrease in the rate of azide binding. As shown in Figure 2, the Thr^{68} hydroxyl group in ferric myoglobin is well placed to make an additional hydrogen bond with the coordinated water molecule. This interaction stabilizes the bound water molecule and results in marked decreases in the association rate and equilibrium constants for azide binding.

As described in the introduction, we hoped to increase the O_2 affinity of pig myoglobin by placing a second hydrogen-bonding donor adjacent to the bound ligand. To our initial disappointment, the Thr^{68} mutation actually caused a 17-fold decrease in K_{O_2}. This was particularly surprising since the results for azide binding, together with the structural data, showed clearly that water coordinated to the ferric iron was stabilized by the β-hydroxyl group. The crystal structure of the ferric protein however, provides a simple explanation for this apparent contradiction. As shown in Figure 2, the hydroxyl group of Thr^{68} is within hydrogen-bonding distance of the main-chain carbonyl oxygen atom of residue 64 and the oxygen atom of the coordinated water molecule. The O–H bond of Thr^{68} is presumably pointed toward the carbonyl oxygen since this atom can only act as a hydrogen-bond acceptor. This requires that the nonbonded electron pairs of the β-hydroxyl group occupy orbitals that point toward the bound ligand. This orientation stabilizes coordinated H_2O, which can act as a donor of a hydrogen atom to the Thr^{68} hydroxyl and as an acceptor of a hydrogen atom from the imidazole side chain of His^{64}. In contrast, bound O_2 has a partial negative charge and can act only as a hydrogen-bond acceptor. As a result, the oxy form of the mutant protein is destabilized relative to the wild-type myoglobin since the negative portions of the hydroxyl and Fe–O_2 dipoles are juxtaposed. In addition to these unfavorable electrostatic interactions, the Thr^{68} side chain could also compete with the bound O_2 for hydrogen bonding to the imidazole side chain of His^{64}. Both effects would be expected to increase the observed rate of thermal O_2 dissociation. The large increase in the CO dissociation rate constant for the mutant protein suggests that the Fe–CO bond is also destabilized by the dipole moment of the E11 β-hydroxyl group (Tables I and V).

In addition to direct interactions with the bound ligand, Thr^{68} also inhibits O_2 binding by stabilizing noncovalently bound water in the distal pocket of ferrous myoglobin. The geminate recombination parameters in Tables III–VI divide the overall binding process into two steps, movement into the distal cavity (X to C in eq 2), and iron–ligand bond formation (C to A). The Val^{68} to Thr mutation caused a decrease in the equilibrium constant for the noncovalent binding of all four ligands, with the greatest effect being a 27-fold decrease in K_{XC} for O_2 binding. The latter effect and the 60-fold reduction in the rate of azide binding may have a common structural cause. Ligand movement into the distal pocket requires the net displacement of water which, in the case of ferrous deoxymyoglobin, is associated with the distal histidine and not directly coordinated to the iron atom (Phillips, 1981; Rohlfs et al., 1989; Carver et al., 1990). This displacement is inhibited by the β-OH of Thr^{68}, which forms additional hydrogen bonds with the distal pocket water molecules. More complete interpretations of these results will require determination of the high-resolution structures of the deoxy and liganded ferrous forms of the Thr^{68} mutant.

In contrast to the diatomic gases, the noncovalent binding of isocyanides is greatly restricted by steric interactions in the heme pocket. For example, the K_{XC} value for methyl isocyanide binding to native myoglobin is small compared to that for the gases (0.01–0.03 M^{-1} vs 2–3 M^{-1}, respectively; Tables IV–VI) and increases markedly when His^{64} and Val^{68} are replaced with smaller amino acids (Carver et al., 1990). Thus, it is reasonable that the isosteric Val^{68} to Thr substitution should produce a smaller effect on the equilibrium constant for isocyanide entry into the distal cavity.

Comparisons with Distal Histidine Mutants of Sperm Whale Myoglobin. Gibbs free energy level diagrams for O_2 binding to wild-type and Thr^{68} pig myoglobin were constructed with use of the rate parameters listed in Table IV in order to compare our results with those observed for His^{64} mutants of sperm whale myoglobin by Carver et al. (1990). The free energy of the Mb + X state was defined as 0, and those for wells C and A were computed as $G_C = -RT \ln K_{XC}$ and $G_A = -RT \ln K$, where K is the overall association equilibrium constant. The observed geminate rate constants were defined as $k_{CA} = A_{CA} \exp(-\Delta G^{\ddagger}_{CA}/RT)$ and $k_{CX} = A_{CX} \exp(-\Delta G^{\ddagger}_{CX}/RT)$, where $\Delta G^{\ddagger}_{CA} = G^{\ddagger}_{CA} - G_C$, $\Delta G^{\ddagger}_{CX} = G^{\ddagger}_{CX} - G_C$, and $G^{\ddagger}$ is the free energy of the kinetic barrier. Both preexponential factors, A_{CA} and A_{CX}, were set equal to 10^{10} s^{-1} so that the differences between the values of k_{CA} and k_{CX} would be expressed solely in the $\Delta G^{\ddagger}$ terms. The meaning and limitations of these definitions have been described by Carver et al. (1990). Our barrier representation differs from that of Frauenfelder and co-workers (Austin et al., 1975), who used Arrhenius expressions and the temperature dependence of the observed rate constants to separate enthalpic and entropic terms [i.e., $k = A \exp(-\Delta H^{\ddagger}/RT)$, where in this case A contains a frequency factor and an $\exp(\Delta S^{\ddagger}/T)$ term]. The barriers in Figure 5 are expressed in terms of Gibbs free energy changes and contain both enthalpic and entropic contributions.

As shown in Figure 5A, replacement of Val^{68} with Thr raises both kinetic barriers for O_2 binding by roughly 0.8 kcal/mol

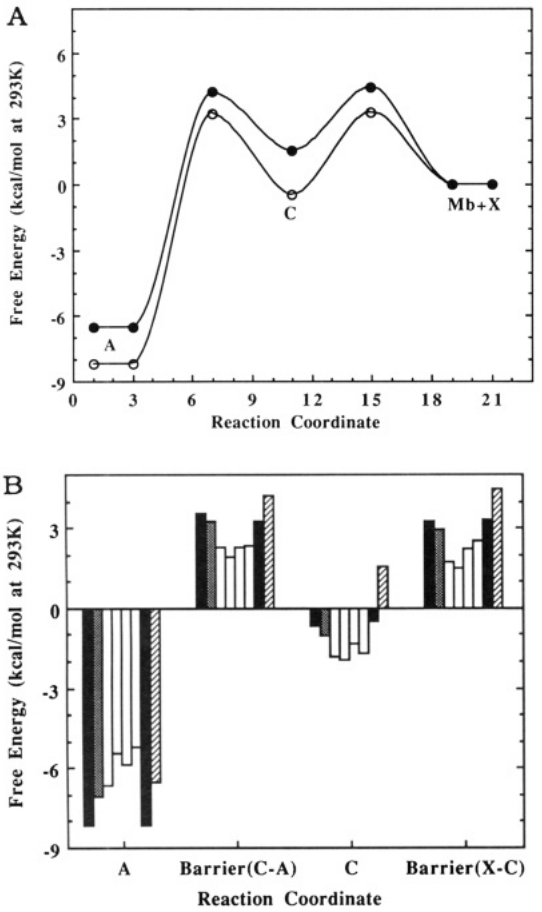

FIGURE 5: (A) Free energy diagrams for oxygen binding to mutant and wild-type pig myoglobin at 20 °C, pH 7. States A, C, and Mb + X correspond to those defined in eq 2. The reaction coordinate numbering is arbitrary and does not imply real distances. The free energy values for the barriers were computed as described in the text and are represented by open circles for the Val^{68} (wild type) and filled circles for the Thr^{68} mutant. The curved lines were generated by interpolation. (B) Comparisons of free energy diagrams for O_2 binding to position 64 (E7) mutants of sperm whale myoglobin and Thr^{68} pig myoglobin. A bar graph format was used to compare the free energy values of all the barriers and states except that for Mb + X, which was defined as zero for all the proteins. From left to right the values refer to wild type (solid bar), Gln^{64} (shaded), Gly^{64}, Val^{64}, Leu^{64}, and Phe^{64} (open bars) sperm whale myoglobins, and wild type (solid bar) and Thr^{68} (hatched bar) pig myoglobins. The sperm whale data were taken from Carver et al. (1990).

but the largest effect is a 1.6 kcal/mol increase in the free energy of the noncovalently bound ligand, state C. The net result is an increase in the rate constants for both O_2 rebinding and escape since both $\Delta G^{\ddagger}_{CA}$ and $\Delta G^{\ddagger}_{CX}$ are decreased substantially. Similar conclusions can be drawn for methyl and ethyl isocyanide binding, although the barrier diagrams are complicated by the presence of two C states.

The effects of the Val^{68} to Thr mutation on O_2 binding to pig myoglobin are compared in Figure 5B to those observed for mutations of His^{64} in sperm whale myoglobin. These free energy barrier diagrams indicate how the polarity of the distal pocket affects oxygen binding. In wild-type pig and sperm whale myoglobins, the only polar residue in the ligand binding site is the distal histidine. Replacing His^{64} with Gly, Val, Leu, and Phe uniformly lowers both kinetic barriers and the free energy of the noncovalently bound ligand, well C in Figure 5B, regardless of the size of the mutated amino acid. This effect has been interpreted in terms of destabilization or loss of distal pocket water molecules, which inhibit the rate of ligand entry into wild-type myoglobin (Carver et al., 1990). Substitution of Gln for His^{64} had a much smaller effect on the kinetic barriers and well C, presumably because the amide group can still stabilize water in the distal cavity. Interpretation of the effects of the Val^{68} to Thr substitution is unambiguous since the mutant protein is isosteric with wild-type pig myoglobin (Figures 1 and 2). The results for this mutation provide convincing positive evidence for the importance of polar interactions since both kinetic barriers and the free energy of noncovalently bound ligands (state C) are raised substantially by the presence of the Thr^{68} hydroxyl group. Thus, there is no doubt that the distal pocket water molecules and their interactions with adjacent amino acid side chains comprise a major portion of the kinetic barrier for ligand entry into deoxymyoglobin.

ACKNOWLEDGMENTS

We are grateful to Szymon Krzywda and Robert Brantley for experimental contributions, Glaxo, U.K., Ltd. for computational time on the ALIANT FX40, and Drs K. Petratos and K. S. Wilson at the EMBL outstation at DESY, Hamburg, FRG, for assistance during X-ray data collection and processing.

Registry No. MNC, 593-75-9; ENC, 624-79-3; nPNC, 627-36-1; nBNC, 2769-64-4; L-Val, 72-18-4; L-Thr, 72-19-5; O_2, 7782-44-7; CO, 630-08-0; NO, 10102-43-9; Fe, 7439-89-6; azide, 14343-69-2; heme, 14875-96-8.

REFERENCES

Austin, R. H., Beeson, K. W., Eisenstein, L., Frauenfelder, H., & Gunsalus, I. C. (1975) *Biochemistry 14*, 5355–5373.

Bolognesi, M., Cannillo, E., Ascenzi, P., Giacometti, G. M., Merli, A., & Brunori, M. (1982) *J. Mol. Biol. 158*, 305–315.

Bolognesi, M., Onesti, S., Gatti, G., Coda, A., Ascenzi, P., & Brunori, M. (1989) *J. Mol. Biol. 205*, 529–544.

Brunger, A. T. (1988) *J. Mol. Biol. 203*, 803–816.

Carver, T. E., Rohlfs, R. J., Olson, J. S., Gibson, Q. H., Blackmore, R. S., Springer, B. A., Egeberg, K. D., & Sligar, S. G (1990) *J. Biol. Chem. 265*, 20007–20020.

Carver, T. E., Olson, J. S., Smerdon, S. J., Krzywda, S., Wilkinson, A. J., Gibson, Q. H., Blackmore, R. S., Dez Ropp, J., & Sligar, S. G. (1991) *Biochemistry 30*, 4697–4705.

Case, D. A., & Karplus, M. (1979) *J. Mol. Biol. 132*, 343–368.

CCP4 (1986) *A Suite of Programs for Protein Crystallography*, SERC Daresbury Laboratory, Warrington, England, U.K.

Dodson, G. G., Hubbard, R. E., Oldfield, T. J., Smerdon, S. J., & Wilkinson, A. J. (1988) *Protein Eng. 2*, 233–237.

Doster, W., Beece, D., Bowne, S. F., DiIorio, E. E., Eisenstein, L., Frauenfelder, H., Reinisch, L., Shyamsunder, E., Winterhalter, K. H., & Yue, K. T. (1982) *Biochemistry 21*, 4831–4839.

Egeberg, K. D., Springer, B. A., Sligar, S. G., Carver, T. E., Rohlfs, R. J., & Olson, J. S. (1990) *J. Biol. Chem. 265*, 11788–11795.

Elber, R., & Karplus, M. (1990) *J. Am. Chem. Soc. 112*, 9161–9175.

Giacometti, G. M., Ascenzi, P., Bolognesi, M., & Brunori, M. (1981a) *J. Mol. Biol. 146*, 363–374.

Giacometti, G. M., Ascenzi, P., Brunori, M., Rigatti, G., Giacometti, G., & Bolognesi, M. (1981b) *J. Mol. Biol. 151*, 315–319.

Gibson, Q. H., Olson, J. S., McKinnie, R. E., & Rohlfs, R. J. (1986) *J. Biol. Chem. 261*, 10228–10239.

Hendrickson, W. A., & Konnert, J. H. (1979) in *Biomolecular Structure, Conformation, Function, and Evolution* (Srinivasan, R., Ed.) Vol. 1, pp 43-57, Pergamon, New York.
Henry, E. R., Sommer, J. H., Hofrichter, J., & Eaton, W. A. (1983) *J. Mol. Biol. 166*, 443-451.
Johnson, K. A., Olson, J. S., & Phillips, G. N. (1989) *J. Mol. Biol. 207*, 459-463.
Jones, T. A. (1978) *J. Appl. Crystallogr. 11*, 268-272.
Jongeward, K. A., Magde, D., Taube, D. J., Marsters, J. C., Traylor, T. G., & Sharma, V. S. (1988) *J. Am. Chem. Soc. 110*, 380-387.
Kabsch, W. (1988) *J. Appl. Crystallogr. 21*, 67-71.
Kottalam, J., & Case, D. A. (1988) *J. Am. Chem. Soc. 110*, 7690-7697.
Kuriyan, J., Wilz, S., Karplus, M., & Petsko, G. A. (1986) *J. Mol. Biol. 192*, 133-154.
Mathews, A. J., Rohlfs, R. J., Olson, J. S., Tame, J., Renaud, J.-P., & Nagai, K. (1989) *J. Biol. Chem. 264*, 16573-16583.
Mims, M. P., Porras, A. G., Olson, J. S., Noble, R. W., & Peterson, J. A. (1983) *J. Biol. Chem. 258*, 14219-14232.
Nagai, K., & Thøgersen, H.-C. (1984) *Nature 309*, 810-812.
Perutz, M. F., & Matthews, F. S. (1966) *J. Mol. Biol. 21*, 199-202.
Petrich, J. W., Poyart, C., & Martin, J. L. (1988) *Biochemistry 27*, 4049-4060.
Phillips, S. E. V. (1980) *J. Mol. Biol. 142*, 531-554.
Phillips, S. E. V. (1981) *The X-ray Structure of Deoxy-Mb (pH 8.5) at 1.4-Å Resolution*, Brookhaven Data Bank.
Phillips, S. E. V., & Schoenborn, B. P. (1981) *Nature 292*, 81-82.
Remaut, E., Stanssens, P., & Fiers, W. (1981) *Gene 15*, 81-93.
Ringe, D., Petsko, G. A., Kerr, D. E., & Ortiz de Montellano, P. R. (1984) *Biochemistry 23*, 2-4.
Rohlfs, R. J., Olson, J. S., & Gibson, Q. H. (1988) *J. Biol. Chem. 263*, 1803-1813.
Rohlfs, R. J., Mathews, A. J., Carver, T. E., Olson, J. S., Springer, B. A., Egeberg, K. D., & Sligar, S. G. (1990) *J. Biol. Chem. 265*, 3168-3176.
Shanaan, B. (1983) *J. Mol. Biol. 171*, 31-59.
Smerdon, S. J., Oldfield, T. J., Dodson, E. J., Dodson, G. G., Hubbard, R. E., & Wilkinson, A. J. (1990) *Acta Crystallogr. B46*, 370-377.
Springer, B. A., & Sligar, S. G. (1987) *Proc. Natl. Acad. Sci. U.S.A. 84*, 8961-8965.
Springer, B. A., Egeberg, K. D., Sligar, S. G., Rohlfs, R. J., Mathews, A. J., & Olson, J. S. (1989) *J. Biol. Chem. 264*, 3057-3060.
Traylor, T. G., Koga, N., & Deardruff, L. A. (1985) *J. Am. Chem. Soc. 107*, 6504-6510.
Varadarajan, R., Szabo, A., & Boxer, S. G. (1985) *Proc. Natl. Acad. Sci. U.S.A. 82*, 5681-5684.
Zoller, M. J., & Smith, M. (1983) *DNA 3*, 479-488.

Thermal Unfolding Pathway for the Thermostable P22 Tailspike Endorhamnosidase†

Bao-lu Chen and Jonathan King*
Department of Biology, Massachusetts Institute of Technology, Cambridge, Massachusetts 02139
Received August 23, 1990; Revised Manuscript Received April 1, 1991

ABSTRACT: The conditions in which protein stability is biologically or industrially relevant frequently differ from those in which reversible denaturation is studied. The trimeric tailspike endorhamnosidase of phage P22 is a viral structural protein which exhibits high stability to heat, proteases, and detergents under a range of environmental conditions. Its intracellular folding pathway includes monomeric and trimeric folding intermediates and has been the subject of detailed genetic analysis. To understand the basis of tailspike thermostability, we have examined the kinetics of thermal and detergent unfolding. During thermal unfolding of the tailspike, a metastable unfolding intermediate accumulates which can be trapped in the cold or in the presence of SDS. This species is still trimeric, but has lost the ability to bind to virus capsids and, unlike the native trimer, is partially susceptible to protease digestion. Its N-terminal regions, containing about 110 residues, are unfolded whereas the central regions and the C-termini of the polypeptide chains are still in the folded state. Thus, the initiation step in thermal denaturation is the unfolding of the N-termini, but melting of the intermediate represents a second kinetic barrier in the denaturation process. This two-step unfolding is unusually slow at elevated temperature; for instance, in 2% SDS at 65 °C, the unfolding rate constant is 1.1×10^{-3} s^{-1} for the transition from the native to the unfolding intermediate and 4.0×10^{-5} s^{-1} for the transition from the intermediate to the unfolded chains. The sequential unfolding pathway explains the insensitivity of the apparent T_m to the presence of temperature-sensitive folding mutations [Sturtevant, J. M., Yu, M.-H., Haase-Pettingell, C., & King, J. (1989) *J. Biol. Chem. 264*, 10693-10698] which are located in the central region of the chain. The metastable unfolding intermediate has not been detected in the forward folding pathway occurring at lower temperatures. The early stage of the high-temperature thermal unfolding pathway is not the reverse of the late stage of the low-temperature folding pathway.

Efforts to understand the stability of the native states of proteins have concentrated on small globular proteins which display reversible unfolding/refolding transitions in denaturant solutions (Schellman, 1987; Goldenberg, 1988; Alber, 1989; Pace, 1990). Under more realistic conditions, for example, under physiological conditions, denaturation is often rapidly followed by aggregation and is not reversible (Wetzel et al., 1990; Volkin & Klibanov, 1989; Mitraki & King, 1989).

† This work was supported by NIH Grant GM17980 and NSF Engineering Research Center Initiative Grant ECD 8803014 to the MIT Biotechnology Process Engineering Center.
* To whom correspondence should be addressed.

0006-2960/91/0430-6260$02.50/0